Proceedings of the Seventh International Conference on
Railway Technology: Research, Development and Maintenance
Edited by: J. Pombo
Civil-Comp Conferences, Volume 15, Paper 17.12
Civil-Comp Press, Edinburgh, United Kingdom, 2026
ISSN: 2753-3239, doi: 10.4203/ccc.15.17.12

Instrumented Wheelset on the KTH Roller Rig: A Feasibility Study with Finite Element Analysis

P. Damsongsaeng[1], M. V. D. Heijden[2], J. F. W. Leung[1] and A. Qazizadeh[1]

[1]Department of Engineering Mechanics, KTH Royal Institute of Technology, Stockholm, Sweden
[2]Fontys University of Applied Sciences, Netherlands

Abstract

Wheel-rail contact forces are essential in understanding the dynamic behaviours of rail vehicles. Despite the difficulty in obtaining direct measurement of these forces, instrumented wheelset technology is a solution to estimate forces through deflection of bodies subjected to forces. This technology can be helpful to validate the dynamic behaviour of the KTH scaled-down roller rig; however, it presents several challenges due to the mechanical arrangement and range of forces. This paper presents the pilot study of the instrumented wheelset on the KTH scaled roller rig with finite element analysis considering vertical and lateral forces. Finite element analysis with a half wheelset model is used to determine sensor locations and evaluate bridge configurations. Later, the developments of a test bench and measurement system are also discussed as a future step towards the realisation of this technology on the KTH scaled roller rig. In addition, practical considerations and alternative solutions are also discussed as a guideline to implement the instrumented wheelset.

Keywords: scaled roller rig, instrumented wheelset, wheel-rail contact forces, finite element analysis, rail vehicle, measurement system.

1 Introduction

Wheel-rail forces are crucial in understanding the dynamic behaviour of vehicles and running gears [1]. Several techniques can be used to obtain these forces, e.g., instrumented rail or trackside measurement, instrumented wheelset, and indirect measurement of forces measured between axlebox and bogie frame or estimation techniques from indirect measurements [2]. Instrumented wheelset technology (IWS), which was first developed in 1955, has been widely used to measure these forces in field tests for vehicle verification and acceptance [3]. An instrumented wheelset is equipped with sensors to measure strains on the wheelset due to forces from wheel-rail contacts and suspension components. Thus, strains can be reconstructed into wheel-rail forces in which both discrete and continuous measurements are possible. Strain gauges which are often used in an instrumented wheelset can be attached to several locations on the wheelset such as the axle [4], wheel web and measuring holes. One of the common approaches is to instrument a wheelset on the wheel web using a strain gauge measurement. This approach provides several advantages including low contribution of inertial forces on the measuring forces and higher bandwidth to capture dynamic behaviour as measuring locations are close to forces [5].

Scaled roller rig has been used in rail vehicle research and development since the 1970s [6,7]. Despite a full-scale test rig providing a better mimic of real conditions, a scaled-down rig enables the possibility to study rail vehicles at low costs, high adjustability, and better environmental control in a laboratory. The Rail Vehicles research group at KTH Royal Institute of Technology has been developing the KTH Scaled Roller Rig, a testing facility for the experimental study of railway running gears, for both research and educational purposes. The scaled roller rig is designed with modular concepts in which both 1/4 and 1/5 scaled-down running gears are possible. To enable the possibility of performing a wide range of vehicle configurations, mechanical arrangements such as wheel-rail combinations, gauges and suspension elements can be adjusted. The roller rig is currently in the instrumentation phase of a single wheelset where various sensors and measurements have been instrumented for verification and validation. Hence, knowledge of wheel-rail forces is not only crucial for cross-validation of the system but also useful in understanding the vehicle dynamics of test subjects.

An instrumented wheelset can enhance the capability of a scaled roller rig as a facility for testing and verification of rail vehicles. This technology has been applied in a scaled roller rig [8] and a scaled rail vehicle [9]. However, it is challenging to introduce an instrumented wheelset to a scaled-down roller rig due to dimension scaling, force range and sensor placement while the material property is similar to the actual wheelset. Kalivoda and Bauer proposed the instrumentation of the roller for the roller rig at the Czech Technical University (CTU roller rig) as its diameter is larger than the wheel [8]. They also considered the axlebox forces measurement as an alternative to estimate contact forces.

Thus, this study emphasises the development of the instrumented wheelset on the KTH scaled roller rig. This focuses on a feasibility study of such technology by using finite element analysis (FEA). Later, the preparation of the instrumentation and testing will be discussed along with technical considerations.

2 KTH Roller rig

The KTH Roller rig serves as a test rig for the experimental study of rail vehicles. This rig has been developing since 2020 when it was first commissioned in autumn 2023. It is capable of simulating three different scenarios: tangent track, curved track, and tangent track with vertical track irregularities. It is possible to configure the system to test in 1/4 and 1/5 scales. The first phase comprises a single suspended wheelset over one roller set for testing on a tangent track, where the length scaling factor (φ_l) of five is used for the current setup. The current wheel-rail combination is a scaled S1002 wheel and 60E1 rail with 1:20 rail inclination. Figure 1 illustrates the major components of the KTH roller rig and installation in the laboratory with sensors.

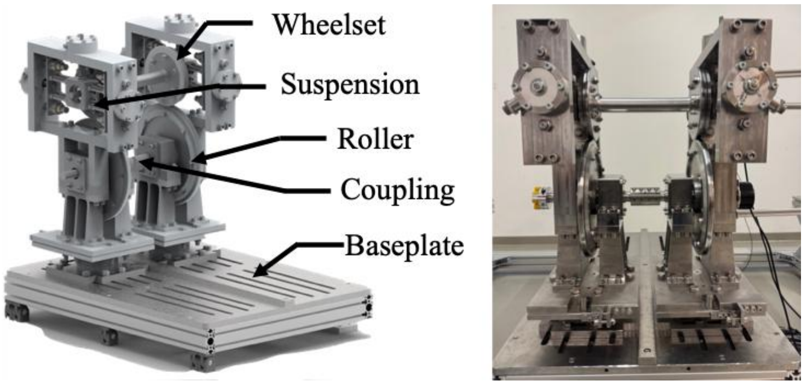

Figure 1: KTH Scaled roller rig.

To obtain the dynamic behaviour of a railway vehicle, the scaling factors must be applied to maintain dynamic similarities. The KTH roller rig employs the DLR scaling method [10] in which a unitary scaling of acceleration (φ_a) is applied. One of the challenges in a scaled-down rig is the density scaling factor. Unlike the density scaling of 0.5 in the DLR method, the KTH roller rig uses a density scaling factor (φ_ρ) of one. Hence, Table 1 summarises some of the important scaling factors, especially in the force-deflection relationship.

Scaling factor	Value
Length (φ_l)	5
Acceleration (φ_a)	1
Density (φ_ρ)	1
Force (φ_F)	125
Stress (φ_σ)	5
Strain (φ_ϵ)	5

Table 1: Selected scaling factors for KTH Roller Rig.

The rig has been instrumented with several sensors to measure important quantities including suspension forces, wheelset displacements in lateral and longitudinal, axlebox acceleration in three directions, and rotational speed for both roller and wheelset. Knowledge of wheel-rail contact forces would allow us to investigate dynamic behaviours in depth and cross-validate experimental and multibody dynamic results. Thus, the real-time wheel-rail contact force measurement/estimation is required to enable such a validation.

3 Instrumented wheelset on the scaled roller rig

In this section, the technique for instrumented wheelset technology is discussed. One of the techniques for the instrumented wheelset is to measure deflections of the wheel web, which is mainly considered in this paper. This method uses strain gauges applied to the wheel web to measure deflection and can then be estimated into wheel-rail contact forces. Since forces are applied on the wheel thread, the measurement location is close to the contact points, which means that the effect of inertial forces would be lower compared to the measurement on the axle. It is also able to detect dynamic phenomena with higher bandwidth [5].

3.1. Wheel-rail forces and method for instrumented wheelset

Wheel-rail contact forces comprise vertical, lateral and longitudinal components. The combination of these forces highly depends on wheel-rail contact situations and operation conditions. In this study, vertical (Q) and lateral (Y) forces are in focus for a feasibility study of instrumented wheelset technology on the scaled roller rig. It is also assumed that there is only one contact point and these contact forces are loaded at the wheel tread as shown in Figure 2, so the effect of lateral contact position is not considered in this study.

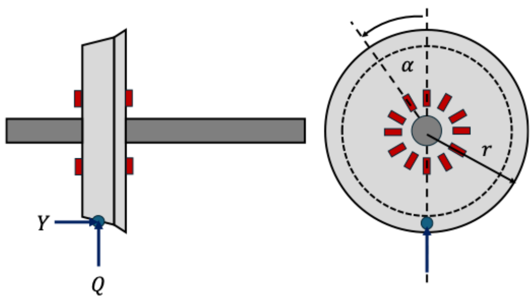

Figure 2: Wheel-rail forces

Considering two forces in Figure 2, the vertical force results in compressive stress and strain on both sides of the wheel, while the lateral force causes bending of the wheel web. Thus, bending due to lateral force (with the given direction in the figure) causes compressive strain on the internal wheel web and extensional strain on the external surface of the wheel web, as summarised in Figure 3. Assuming a linear system, the relationship between force and strain can be written in the form of a linear combination as

$$\boldsymbol{\varepsilon} = \boldsymbol{\beta} Y + \boldsymbol{\gamma} Q. \quad (1)$$

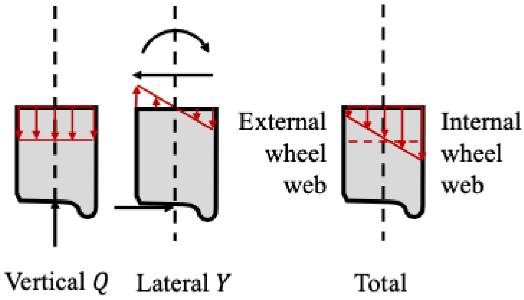

Figure 3: Strains due to vertical and lateral forces

In this study, strains on internal and external wheel web surfaces are examined. As the relationship between force and strain can be given as a linear relationship, strains on the internal and external surfaces of a wheel web, i.e. ε_i and ε_o can be expressed in matrix form as

$$\boldsymbol{\varepsilon} = \boldsymbol{S}\boldsymbol{F}, \quad (2.1)$$

$$\begin{bmatrix} \varepsilon_i \\ \varepsilon_e \end{bmatrix} = \begin{bmatrix} s_{Qi} & s_{Yi} \\ s_{Qe} & s_{Ye} \end{bmatrix} \begin{bmatrix} Q \\ Y \end{bmatrix}, \quad (2.2)$$

where $\boldsymbol{S}$ is the sensitivity matrix. To determine forces from measured strains, Eq. 2.1 can be reformulated by using the inverse of the sensitivity as

$$\boldsymbol{F} = \boldsymbol{S}^{-1}\boldsymbol{\varepsilon} = \boldsymbol{A}\boldsymbol{\varepsilon}, \quad (3)$$

where $\boldsymbol{A}$ is a so-called calibration matrix which is the inverse of $\boldsymbol{S}$. This calibration Metrix can be calculated from a set of tests, where forces and strains are obtained, by using the Moore-Penrose pseudo-inverse matrix which is given as

$$\boldsymbol{A}^* = \boldsymbol{F}\boldsymbol{\varepsilon}^T(\boldsymbol{\varepsilon}\boldsymbol{\varepsilon}^T)^{-1}. \quad (4)$$

To solve this linear system, two independent signals are required. So, we focus on one measurement on the internal surface of the wheel web and one measurement on the external surface of the wheel web.

3.2. Finite element analysis

To determine the wheel web deflections due to wheel-rail forces, the Finite element model (FEM) is implemented using a half-wheelset model with a general mesh size of 1.8 mm. The half-wheelset consists of three parts: a wheel mount, wheel rim, and half an axle as shown in Figure 4 (left). In this case, wheel mounts are considered as wheel webs. These components are made of structural steel with a Young's modulus (E) of 200 GPa and the Poisson's ratio (ν) of 0.3. The modular design of wheelset structure allows us to replace wheel rims with different profiles; however, it can be challenging to create the finite element model due to its complexities. Thus, the finite element model is created with the wheel mount, wheel rim, and axle merged into a single component in which there is no additional degree of freedom (DOF) between the different bodies. Due to the symmetry in the wheelset, a half model is simulated with symmetric boundary conditions at the midplane of the wheelset. Since the loads for the scaled roller rig are much lower than the actual rail vehicle, only elastic behaviour is considered.

The realistic range of forces is considered by using the force scaling factor mentioned in Table 1. The range of vertical forces consists of 400, 520, and 640 N, which correspond to actual vertical wheel loads of 50, 65, and 80 kN respectively. In addition, four lateral force levels are 80, 120, 160, and 200 N, which are equivalent to 10, 15, 20, and 25 kN in full-scale. These ranges cover possible vehicles that can operate on the KTH roller rig. Figure 4 (right) illustrates the directions for vertical and lateral forces considered in this study.

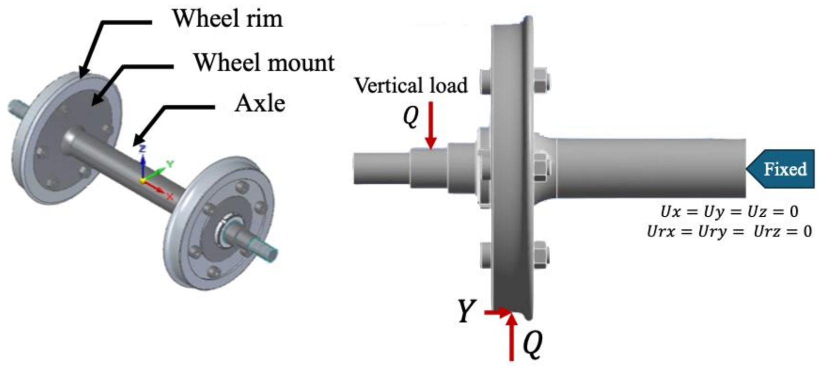

Figure 4: Wheelset (left) and finite element model and boundary conditions (right).

4 Radial strains due to wheel-rail forces

In this section, deformations of a wheel web subjected to various ranges of vertical and lateral forces are investigated by means of finite element analysis. As mentioned earlier, radial strains are measured on the wheel web resulted from load application on the wheel tread.

4.1 Radial strains due to lateral forces

In the initial step, the suitable radial position for strain gauge placement is studied by considering radial strain at different radial positions (r) when a half-wheelset is subjected to the lateral force of 120 N. The possible radial position on the internal wheel web ranges between 30 and 50 mm, while the radial position in the range of 30 to 42 mm is considered for the outer surface due to the limited space on the wheel mount.

Figure 5 shows radial strains as a function of rotational angle (α) at different radial positions (r) for measurements on both internal and external surfaces. It can be seen that the radial position of 30 mm (near the axle) gives the highest sensitivity to the lateral force due to the higher bending moment caused at that section. This position is therefore suitable for placing strain gauges. At this position, the magnitude of strain on the internal surface is also similar to that on the external surface. Magnitude differences of strain are caused by the distance between the load point and the neutral axis and the complex geometry of the wheel mount. As these strains are caused by bending, compressive and extensional strains are observed at the internal and external surface respectively, as discussed in Section 3.1.

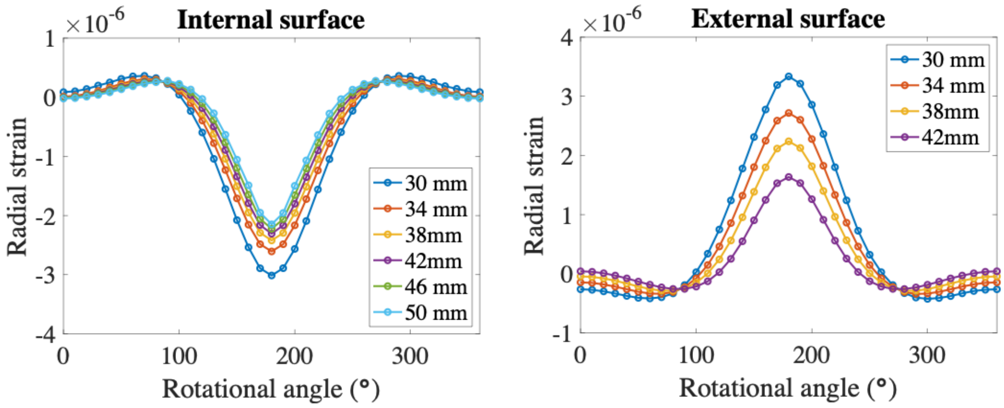

Figure 5: The relationship between rotational angles and radial strains on the internal (left) and external (right) surfaces with the lateral force of 120 N at different radial positions.

Then, four lateral force levels are applied to the wheel tread to study the behaviour of strain reading on internal and external surfaces at 30 mm. Figure 6 illustrates the results of radial strains under different lateral loads on both surfaces. The magnitude of strain changes linearly with the magnitude of lateral force due to elastic material behaviour.

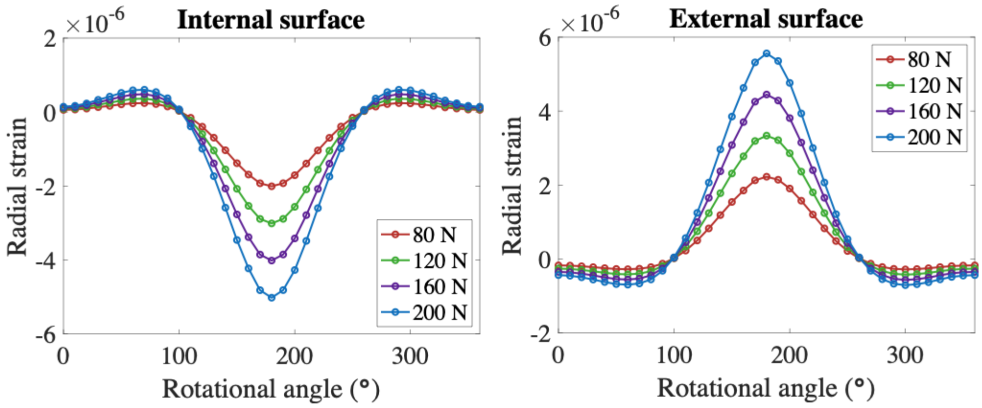

Figure 6: Radial strains on the internal (left) and external (right) surfaces at a radial position of 30 mm.

4.2 Radial strain due to vertical forces

In this subsection, the radial strain at 30 mm due to vertical force is investigated for both internal and external surfaces. There are three vertical force levels, including 400, 520, and 640 N. The results in Figure 7 provide a comparison between radial strains on the internal and external surfaces due to vertical force. Vertical force causes compressive strain on both surfaces, as shown in Figure 3; however, the range of strain on the external surface is higher than the range of strain on the internal surface due to the boundary condition of vertical load at the axle. Radial strain due to vertical force is generally lower than that due to lateral force.

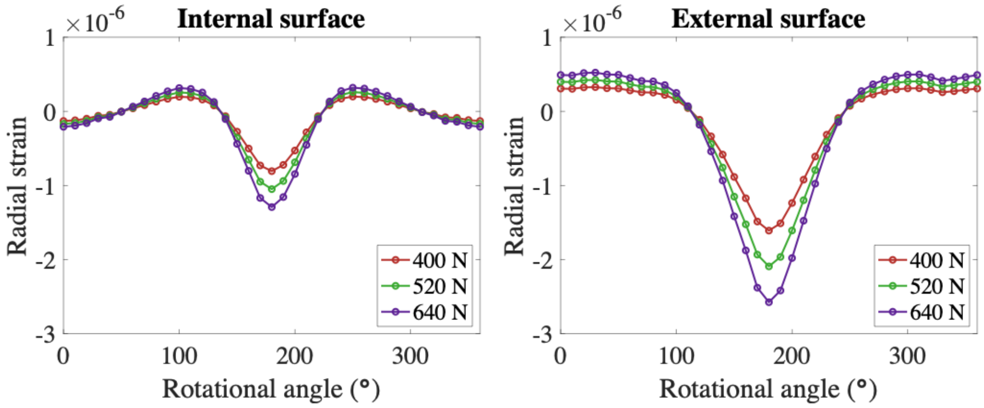

Figure 7: Radial strain at a radial position of 30 mm for both internal (left) and external (right) surfaces under three vertical forces.

4.3 Radial strains of combined loads

To observe the complex loading of wheel-rail forces, radial strain due to combined vertical and lateral forces is presented and discussed in this subsection. Two combinations are considered, including a lateral force of 120 N with a vertical force of 400 N and a lateral force of 160 N with a vertical force of 520 N. Both combinations give the derailment coefficient (Y/Q) ratio of 0.3.

Results of radial strain for the first combination are given in Figure 8. When both lateral and vertical forces are applied, the resultant radial strain is the sum of the radial strain from the lateral force and the radial strain from the vertical force. This is the effect due to the superposition principle. Hence, the magnitude of radial strain at 30 mm on the internal surface is higher than that on the external surface, but lower for the external surface due to the compressive strains from the lateral loading.

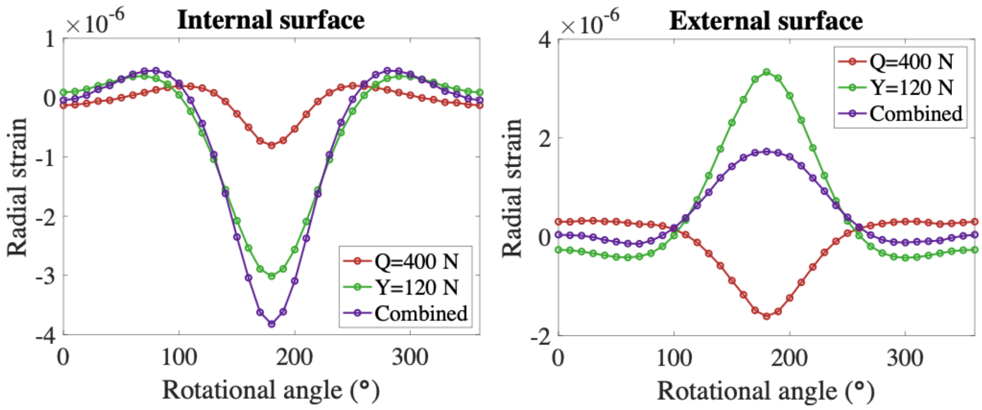

Figure 8: Radial strains on the internal (left) and external (right) surfaces of the wheel web when subjected to vertical force of 400 N and lateral force of 120 N.

Results in Figure 9 show the radial strain from the second combined load. The results show that the loading is within the elastic region and that the general behaviour of the combined radial strains is similar to the first combination. The difference is that the radial strain magnitude from this load combination is higher than that of the first combination linearly.

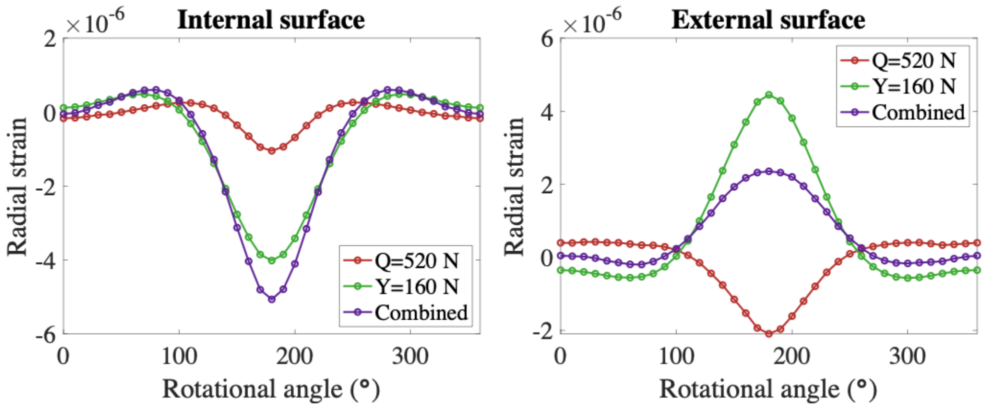

Figure 9: Radial strains on the internal (left) and external (right) surfaces of the wheel web when subjected to vertical force of 520 N and lateral force of 160 N.

5 Sensor placement and bridge configuration

To represent the effect of strain gauge dimensions, the virtual strain gauges are implemented in FEM with a size of $3.5 \times 5\ mm^2$ in which the centre of the gauge is at a radial position of 30 mm. The virtual strain gauges are applied to both internal and external surfaces of the wheel. Figure 10 shows the virtual strain gauge placement and Wheatstone bridge configuration per set. A set of 12 strain gauges per bridge is selected to obtain the continuous measurement. Thus, the angle between each strain gauge is 30 degrees. In general, the ratio between output voltage (V_o) and excitation voltage (V_e) is given as

$$\frac{V_o}{V_e} = \frac{R_1}{R_1 + R_2} - \frac{R_4}{R3 + R4}, \tag{5}$$

where R_1, R_2, R_3, and R_4 are the resistances from the serial connection of three strain gauges. The change of resistance of a strain gauge is a function of gauge factor (GF) and strain (ε), i.e. $\Delta R = GF \cdot \varepsilon \cdot R$ where R is initial nominal resistance.

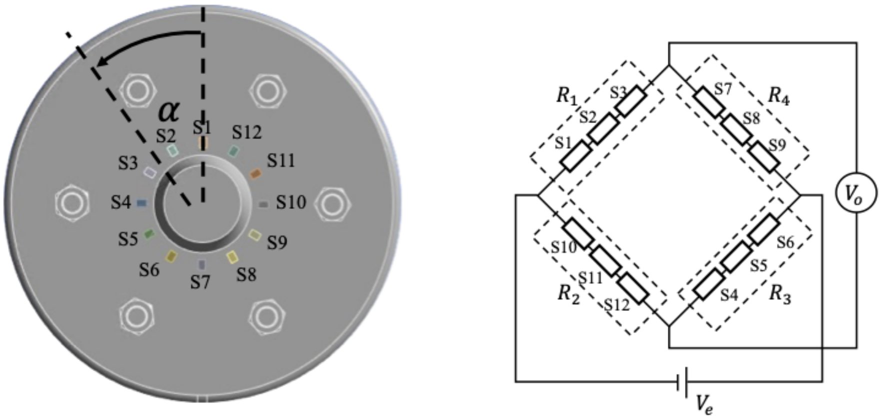

Figure 10: Sensor placement and bridge circuit.

An evaluation of the bridge configuration is performed using the method in [11]. Results are presented in terms of equivalent strains of the chosen bridge configuration. According to the simplification of the Wheatstone bridge, the ratio between the output voltage and the voltage excitation is

$$\frac{V_o}{V_e} = \frac{GF}{N}(\varepsilon_e), \tag{6}$$

where

$$\varepsilon_e = \sum_{i=1}^{3} \varepsilon_{si} - \sum_{j=7}^{9} \varepsilon_{sj} + \sum_{k=4}^{6} \varepsilon_{sk} - \sum_{l=10}^{12} \varepsilon_{sl}.$$

To evaluate the bridge configuration, the combination of a lateral force of 120 N and a vertical force of 400 N is chosen. The effect of strain gauge size is small in comparison to the results in Section 4 as it covers radial strain between positions of 28.25 and 31.75 mm. First, the instrumentation of strain gauges on the external surface is considered. Each bridge consists of 12 strain gauges with 30 degrees between each strain gauge as mentioned earlier. Two schemes are investigated as follows:

1) Two bridges (bridges A and B) with a spacing between each bridge of 90 degrees
2) Three bridges (bridges A, B and C) with the second bridge and third bridge are placed at 60 and 120 degrees from the first bridge.

To evaluate the output of each scheme, the total output is synthesised by means of the root sum of squares (RSS) to combine all bridge outputs.

The comparison between the two schemes is shown in Figure 11. It can be seen that the second scheme gives a higher output compared to the first scheme. In addition, the oscillation of the output for the second scheme is also smaller than that of the first one. However, it requires a higher number of strain gauges, which can pose a system complexity issue for a scaled roller rig. Hence, the first one is chosen.

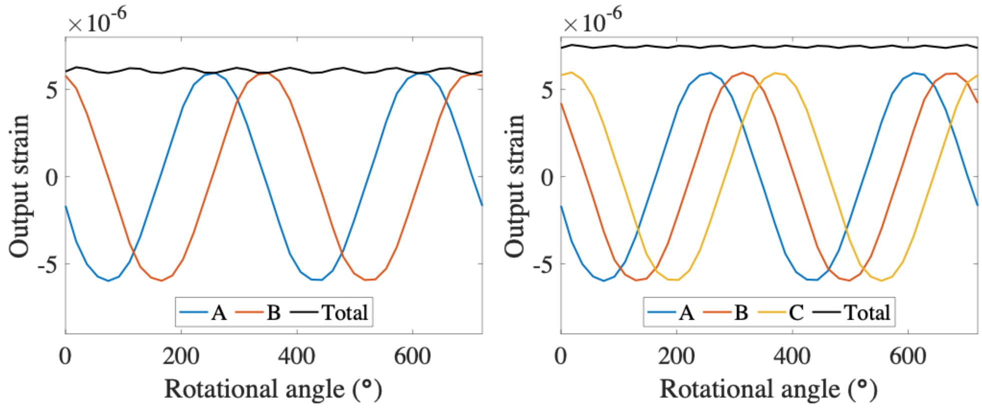

Figure 11: Equivalent strain outputs from bridge circuits on the external surface of wheel web using two (left) and three (right) bridges.

The evaluation of the first scheme is also performed for measurement on the internal surface. As the magnitude of radial strain is higher than that of the external side, the output is also higher as shown in Figure 12; however, the fluctuation is also higher than that of the external side. This can be improved by considering the placement of the sensor at some angle to eliminate a specific harmonic.

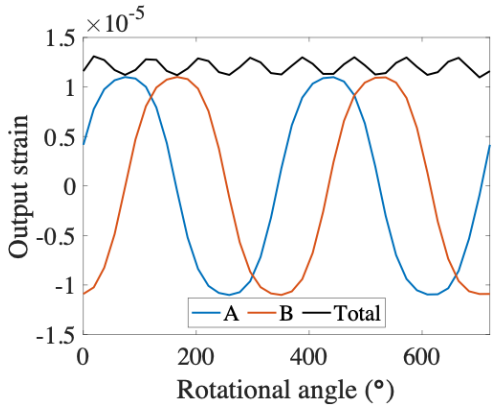

Figure 12: Equivalent strain outputs on the internal surface of wheel web using two bridges with an angle of 90 degrees between the two bridges.

To summarise, the sensor placement and bridge configuration are evaluated for two signals measured on internal and external surfaces. These two signals are important to calculate the calibration matrix to estimate vertical and lateral forces. The strains observed from the finite element analysis and output from the bridge configuration are just above the resolution of normal metallic strain gauges, where the resolution of 0.1-1 με can be obtained. Hence, a strain gauge with a high gauge factor (GF) would be preferred. More importantly, signal conditioning of the measurement system must be considered carefully.

6 Instrumentation preparation and practical consideration

To determine the calibration matrix mentioned in Section 3, both results from finite element analysis and tests are needed. The test bench is prepared for calibration of the instrumented wheelset, where both vertical and lateral forces can be applied and measured through load cells. The static test bench is not only used to obtain results for calculating the calibration matrix, but also for the validation of results from the finite element analysis. This step is crucial for the execution of the instrumented wheelset on the scaled roller rig.

One of the challenges for an instrumented wheelset is data transmission due to sensor placement on rotating bodies. One of the possibilities is to transmit signals through slip ring devices, which have a short life span due to the mechanical degradation of contact parts. More recently, wireless transmission or telemetry is possible with advances in signal processing and transmission [3]. Figure 13 shows schematics of the measurement system planned to be implemented on the scaled roller rig. As the range of strain is much lower than a full-scale system, signal conditioning, including an amplifier and an analog-to-digital converter, must be carefully designed.

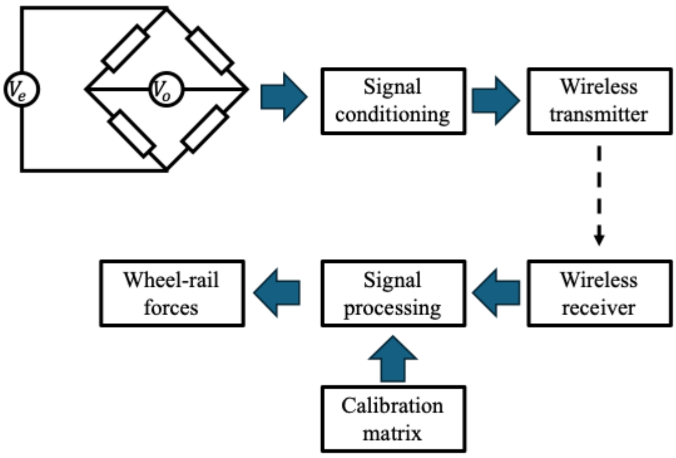

Figure 13: Measurement system with wireless data transmission

6 Conclusions

This paper presents the pilot study of the instrumentation of wheel-rail force measurement on the KTH roller rig, where the wheel hub instrumentation is in focus. This serves as a feasibility study of the application of an instrumented wheelset to estimate wheel-rail force on the scaled roller rig, as they are crucial in testing and verification of the dynamic behaviour of rail vehicles. The study employs finite element analysis of the wheelset to investigate wheel deformation due to vertical and lateral contact forces.

The result of radial strain shows the most suitable radial position at a radius of 30 mm for sensor placement to obtain the highest sensitivity. The sensor placement and bridge configuration are also investigated in which 12 strain gauges are used per bridge. However, the angulation of sensor placement for the optimal position would be further studied to reduce the ripple effects on measured signals. The results from finite element analysis will be used to calibrate the transformation matrix, together with experiments in the iterative calibration process. This is a crucial step to estimate forces through measured deformations. The results from finite element analysis also allow us to take practical implementation into consideration especially in terms of measurement system and signal conditioning.

As the instrument preparation is discussed, experiments will be conducted to validate the results from finite element analysis and to calculate the calibration matrix. Other parameters, such as lateral wheel-rail contact position and longitudinal force, will be further studied.

References

[1] E. Andersson, M. Berg, S. Stichel, "Rail vehicle dynamics", KTH Railway Group, Stockholm, 2014.

[2] P. Wu, F. Zhang, J. Wang, L. Wei, W. Huo, "Review of wheel-rail forces measuring technology for railway vehicles", Advances in Mechanical Engineering, 15, 3, 2023, doi: 10.1177/16878132231158991.

[3] G. Ekdahl, L. Andersson, M. Wrang, "Instrumented wheelset technology—advances and applications", IHHA Specialist Technical Session (STS) Kiruna Sweden, 2007.

[4] G. Cazzulani, E. Di Gialleonardo, S. Bionda, M. Bassetti, P. Crosio, F. Braghin, "A new approach for the evaluation and the improvement of the metrological characteristics of an instrumented wheelset for the measure of wheel–rail contact forces", Proc. Inst. Mech. Eng. F J. Rail Rapid Transit, 231, 4, 381–393, 2017, doi: 10.1177/0954409716631785.

[5] A. Bracciali, F. del Cavaliere, M. Macherelli, "Review of Instrumented Wheelset Technology and Applications", in "Proceeding of the Second International Conference on Railway Technology: Research, Development and Maintenance", J. Pombo, (Editor), Civil-Comp Press, Stirlingshire, UK, Paper 167, 2014.

[6] N. Bosso, P. D. Allen, N. Zampieri, "Scale Testing Theory and Approaches", in "Handbook of Railway Vehicle Dynamics, Second Edition", S. Iwnicki, M. Spiryagin, C. Cole, and T. McSweeney, (Editors), Boca Raton: CRC Press, 825–867, 2019.

[7] A. Jaschinski, H. Chollet, S. Iwnicki, A. Wickens, J. Würzen, "The Application of Roller Rigs to Railway Vehicle Dynamics", Vehicle System Dynamics, 31, 345–392, 1999, doi: 10.1076/vesd.31.5.345.8360.

[8] J. Kalivoda, P. Bauer, "Scaled Roller Rig to Assess the Influence of Active Wheelset Steering on Wheel-Rail Contact Forces", in "Advances in Dynamics of Vehicles on Roads and Tracks", M. Klomp, F. Bruzelius, J. Nielsen, A. Hillemyr, (Editors), Lecture Notes in Mechanical Engineering, Springer, Cham, 82–89, 2020, doi: 10.1007/978-3-030-38077-9_10.

[9] P. Urda, S. Muñoz, J. F. Aceituno, J. L. Escalona, "Wheel-rail contact force measurement using strain gauges and distance lasers on a scaled railway

vehicle", Mech. Syst. Signal Process., 138, Paper 106555, 2020, doi: 10.1016/j.ymssp.2019.106555.

[10] M. Gretzschel, A. Jaschinski, "Design of an Active Wheelset on a Scaled Roller Rig", Vehicle System Dynamics, 41, 5, 365–381, 2004, doi: 10.1080/00423110412331300336.

[11] C. Shuangxi, "A method for evaluating the design scheme of continuous measuring bridge of the instrumented wheelset", Measurement, 239, Paper 115401, 2025, doi: 10.1016/j.measurement.2024.115401.